Journal for ImmunoTherapy of Cancer

Immune system and intestinal microbiota determine efficacy of androgen deprivation therapy against prostate cancer

Safae Terrisse ,[1,2] Anne-Gaelle Goubet,[1] Kousuke Ueda,[3] Andrew Maltez Thomas,[4] Valentin Quiniou,[5] Cassandra Thelemaque,[1] Garett Dunsmore,[1] Emmanuel Clave ,[6] Melissa Gamat-Huber ,[7] Satoru Yonekura,[1] Gladys Ferrere,[1] Conrad Rauber,[1] Hang Phuong Pham,[5] Jean-Eudes Fahrner,[1,8] Eugenie Pizzato,[1] Pierre Ly,[1] Marine Fidelle,[1] Marine Mazzenga,[1] Carolina Alves Costa Silva,[1,8] Federica Armanini,[4] Federica Pinto,[4] Francesco Asnicar,[4] Romain Daillère,[9,10] Lisa Derosa,[1,11] Corentin Richard,[12] Pierre Blanchard,[13] Bertrand Routy,[12,14] Stéphane Culine,[2,15] Paule Opolon,[16] Aymeric Silvin,[1] Florent Ginhoux,[1] Antoine Toubert,[17,18] Nicola Segata ,[4] Douglas G McNeel ,[19] Karim Fizazi ,[8,20] Guido Kroemer,[9,21] Laurence Zitvogel[22,23]

To cite: Terrisse S, Goubet A-G, Ueda K, *et al*. Immune system and intestinal microbiota determine efficacy of androgen deprivation therapy against prostate cancer. *Journal for ImmunoTherapy of Cancer* 2022;**10**:e004191. doi:10.1136/jitc-2021-004191

► Additional supplemental material is published online only. To view, please visit the journal online (http://dx.doi.org/10.1136/jitc-2021-004191).

KF, GK and LZ contributed equally.

KF, GK and LZ are joint senior authors.

Accepted 08 January 2022

For numbered affiliations see end of article.

Correspondence to
Laurence Zitvogel;
laurence.zitvogel@orange.fr

Guido Kroemer;
kroemer@orange.fr

ABSTRACT

Background Prostate cancer (PC) responds to androgen deprivation therapy (ADT) usually in a transient fashion, progressing from hormone-sensitive PC (HSPC) to castration-resistant PC (CRPC). We investigated a mouse model of PC as well as specimens from PC patients to unravel an unsuspected contribution of thymus-derived T lymphocytes and the intestinal microbiota in the efficacy of ADT.

Methods Preclinical experiments were performed in PC-bearing mice, immunocompetent or immunodeficient. In parallel, we prospectively included 65 HSPC and CRPC patients (Oncobiotic trial) to analyze their feces and blood specimens.

Results In PC-bearing mice, ADT increased thymic cellularity and output. PC implanted in T lymphocyte-depleted or athymic mice responded less efficiently to ADT than in immunocompetent mice. Moreover, depletion of the intestinal microbiota by oral antibiotics reduced the efficacy of ADT. PC reduced the relative abundance of *Akkermansia muciniphila* in the gut, and this effect was reversed by ADT. Moreover, cohousing of PC-bearing mice with tumor-free mice or oral gavage with *Akkermansia* improved the efficacy of ADT. This appears to be applicable to PC patients because long-term ADT resulted in an increase of thymic output, as demonstrated by an increase in circulating recent thymic emigrant cells (sjTRECs). Moreover, as compared with HSPC controls, CRPC patients demonstrated a shift in their intestinal microbiota that significantly correlated with sjTRECs. While feces from healthy volunteers restored ADT efficacy, feces from PC patients failed to do so.

Conclusions These findings suggest the potential clinical utility of reversing intestinal dysbiosis and repairing acquired immune defects in PC patients.

INTRODUCTION

Prostate cancer (PC) is the most prevalent malignant disease in men, affecting the vast majority of octogenarians.[1] Driven by a heterogeneous set of oncogenic drivers, PC usually develops in a multistep process from benign hypertrophy through adenoma to adenocarcinoma that first invades local tissues and then disseminates to distant sites.[2] High-risk localized PC is initially treated by radical prostatectomy and/or local radiotherapy, often together with adjuvant androgen deprivation therapy (ADT) by surgical castration (bilateral orchiectomy), chemical castration (subcutaneously injected gonadotropin-releasing hormone receptor agonists) or antiandrogens (orally administered drugs such as abiraterone or enzalutamide that inhibit androgen synthesis or the nuclear translocation of the androgen receptor, respectively).[3] ADT is also the therapy of choice for metastatic hormone-sensitive PC (HSPC). However, after a latency HSPC usually progresses to castration-resistant PC (CRPC), then requiring more toxic treatments including chemotherapy before the final switch to palliative care.[4] Importantly, the prognosis of PC is not only dictated by cancer cell-autonomous alterations. Thus, infiltration of PC by $CD8^+$ cytotoxic T lymphocytes indicates good prognosis, while infiltration by immunosuppressive $CD4^+$ regulatory T cells (Tregs) has a negative prognostic impact.[5–9]

Although the efficacy of targeted therapies (including ADT) and chemotherapies has been usually considered to be mediated by cancer cell-autonomous effects,[10 11] recent work suggests that highly successful molecules usually also affect the cancer-immune dialog, favoring antitumor immune responses.[12 13] This has been well documented for widely used chemotherapeutic agents including single-agent anthracyclines,[14 15] dactinomycin,[16] oxaliplatin,[17] taxanes,[18] as well as specific combination therapies.[19 20] Such agents induce immunogenic cell death, rendering malignant cells recognizable to the immune system.[21] Moreover, multiple targeted agents including tyrosine or serine/threonine kinase inhibitors have been found to enhance immunosurveillance by a plethora of different mechanisms that help explain their long-term effects beyond treatment discontinuation.[13 22 23] This applies as well to estrogen receptor antagonists, which are used for the treatment of hormone receptor-positive breast cancer.[24] Both in preclinical models and in PC patients, ADT causes an increase of the immune infiltrate of the malignant tumor and the adjacent normal prostate[25–29] suggesting that ADT triggers at least a transient immune response, likely against both normal and cancer-specific antigens.[30] Of note, testosterone is one of the best known endogenous accelerators of thymic atrophy,[31 32] suggesting that ADT might reverse thymic aging, which is one of the drivers of T cell aging and the senescence-associated decline in anticancer immunosurveillance.[33] Hence, it is conceivable that ADT has local as well as systemic effects on antitumor immune responses.

It would be naïve to assume that the immune-cancer dialog would not be influenced by external factors. Indeed, recent work by multiple groups has revealed the cardinal importance of the gut microbiota in determining the general immune tonus,[34–36] as well as cross-reactive cancer antigen-specific immune responses.[37 38] Circumstantial evidence indicates that ADT modifies the gut microbiota,[39–41] providing yet another possible mechanism through which ADT might affect PC immunosurveillance.

Driven by the aforementioned considerations, we decided to investigate the effects of ADT on thymic function and the microbiota while addressing the possibility that thymus-derived T cells as well as specific bacterial species might influence the efficacy of ADT against PC. Our preclinical data (in mice) as well as our clinical-translational results (in PC patients) suggest a complex relationship between ADT, gut microbiota, PC and thymic function that has a major impact on the therapeutic outcome of ADT.

MATERIAL AND METHODS

This section will be described in online supplemental file.

RESULTS

T cell-dependent efficacy of ADT in mice with PC

The murine Myc-CaP cell line has an amplified androgen receptor gene and requires testosterone for optimal proliferation.[42] Myc-CaP PCs implanted in syngeneic FVB/N mice respond to androgen depletion therapy (ADT resulting from subcutaneous injection of the gonadotropin-releasing hormone receptor antagonist degarelix acetate)[43] by growth arrest and partial shrinkage. This effect usually lasts 15 to 25 days until cancer growth resumes (figure 1A,B), indicating progression from HSPC to CRPC. Of note, depletion of T lymphocytes by intravenous injection of antibodies depleting $CD4^+$and $CD8^+$ cells attenuated tumor growth control by ADT (figure 1C) and accelerated time to progression (TTP) from HSPC to CRPC (figure 1D). A similar effect was observed when PCs were implanted into mice homozygous for the nude spontaneous mutation (*Foxn1 nu*) that are athymic and hence lack thymus-dependent T lymphocytes. As compared with PCs evolving in immunocompetent mice, PCs established in *nu/nu* mice responded less efficiently to ADT (figure 1E) and progressed more rapidly (figure 1F). Of note, intravenous transfer of thymocytes from FVB/N mice into *nu/nu* mice blunted the natural progression of PCs (figure 1G,H). However, similar to what has been found in PC patients [44 45] immune checkpoint blockade using antibodies targeting CTLA-4 and PD-1 failed to achieve a major improvement of ADT efficacy (online supplemental file 2).

Opposing thymic effects of PC and ADT in mice

Intrigued by the importance of thymus-derived T cells in PC immunosurveillance (see above), we investigated the impact of PC and ADT on the thymus. Histological analysis (figure 2A), followed by morphometric calculations (figure 2B–D) revealed that, as compared with tumor-free mice, mice bearing PCs and receiving sham treatment displayed a reduction of thymic area, in particular the medulla. ADT increased the thymus area, in particular the cortex, thus reversing the effect of PC on the cortical area (figure 2B–D). Immunophenotyping of thymocyte suspensions using immunofluorescence and cytometry unveiled a PC-induced increase in double-negative type-3 (DN3) cells with a $CD4^-CD8^-CD44^-CD25^+$ phenotype that was only partially reversed by ADT. PC also caused a relative increase of double-positive (DP) cells (phenotype: $CD4^+CD8^+$). The relative abundance of single-positive $CD4^+CD8^-$ or $CD4^-CD8^+$ cells, as well as the percentage of $TCR\beta^+$ cells were reduced by PC irrespective of ADT (figure 2E). In the blood, ADT stimulated an increase in the percentage of DN T cells (phenotype: $CD4^-CD8^-CD3^+$), reversed the increase of the $CD4^+/CD8^+$ T cell ratio and tended to attenuate the recirculation of DP cells (figure 2F). In contrast, the PC-induced reduction of $TCR\beta^+$ cells among $CD3^+$ lymphocytes was not corrected by ADT or even worsened it (figure 2F).

Altogether, these results indicate subtle thymotropic effects of ADT that may favor the thymic efflux of DN T cells and reverse the PC-induced increase in the peripheral $CD4^+/CD8^+$ T cell ratio.

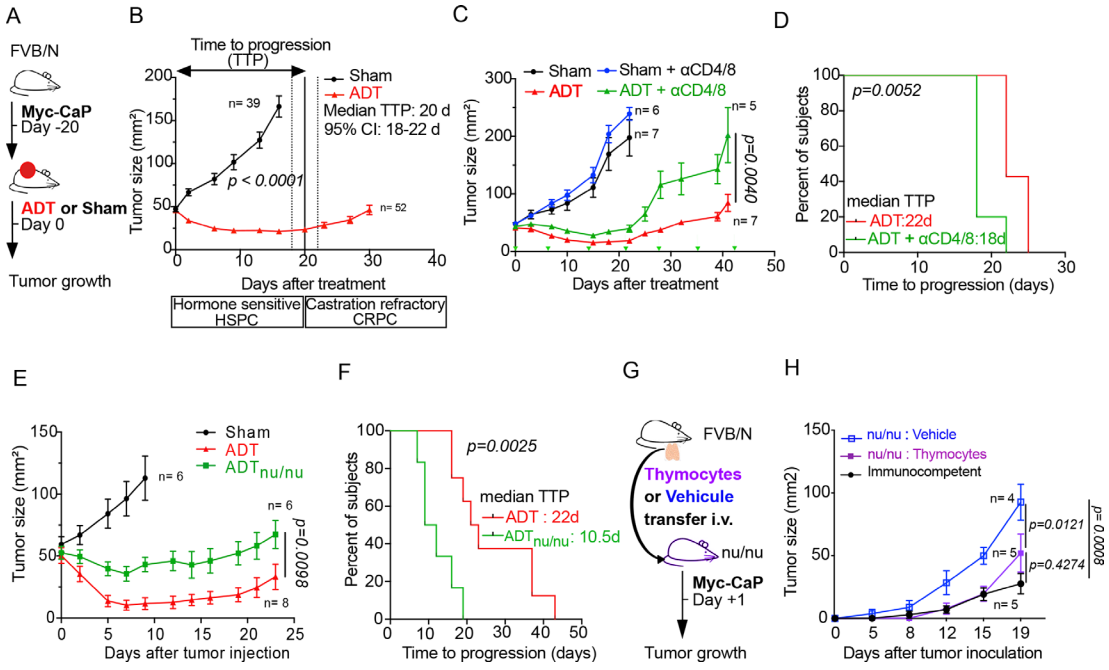

Figure 1 T cell-dependent efficacy of ADT in mice with prostate cancer (PC). (A) Experimental setup to investigate the effect of ADT in Myc-CaP prostate cancer model. (B) Tumor growth curves and representation of TTP defining hormone sensitive (HSPC) and castration resistance (CRPC) intervals. (C) Tumor growth kinetics of Myc-CaP following depletion of T cells using αCD4 and αCD8 monoclonal antibodies, 3 days before systemic therapy (ADT or sham control) and twice a week until sacrifice. (D) Kaplan-Meier curves illustrating TTP. (E, F) Tumor growth kinetics in Myc-CaP bearing *nu/nu* mice, treated with ADT or sham control (E) and TTP Kaplan-Meier curves (F). (G) experimental setup of thymocytes or vehicle transfer from FVB/N healthy mice to *nu/nu* by i.v tail injection before Myc-CaP inoculation the next day. (H) Tumor growth kinetics in the *nu/nu* groups compared with immunocompetent FVB/N mice. ADT, androgen deprivation therapy; TTP, time to progression.

Relationship between ADT and gut microbiota in mice

In the next step, we investigated the relationship between ADT and the intestinal microbiota. Oral supplementation of three broad-spectrum antibiotics (ampicillin, colistin, streptomycin), a combination that eliminates the majority of gut commensals[46] (figure 3A), reduced the anticancer effects of ADT in two different laboratories located in Villejuif, France (figure 3B) and Wisconsin, USA (figure 3C). Hence, independently from its exact composition (which depends on the animal facility), the microflora can support the efficacy of ADT. Of note, comparative 16S ribosomal RNA sequencing of the fecal microbiota from tumor-free and PC-bearing mice revealed a reduction of alpha diversity of the microbiota determined by two different algorithms (figure 3D) with a tangible effect on the overall microbial composition detectable by principal component analyses (figure 3E). Linear discriminant analysis effect size revealed the PC-associated depletion of *Verrucomicrobiaceae* family members including the *Akkermansia muciniphila* species (figure 3F), *Ruminococcaceae* and *Rikenellaceae* (represented by *Alistipes* spp) known to be associated with response to PD1 blockade.[47 48] The comparison of the microbiota of PC-bearing mice receiving ADT or sham treatments indicated that ADT restored richness that is, alpha diversity (figure 3G) and increased the relative abundance of *A. muciniphila* (figure 3H), echoing prior reports that oral antiandrogens, including bicalutamide, enzalutamide and abiraterone acetate increase the abundance of *A. muciniphila* in PC patients.[39 40] Several *Lachnospiraceae* family members were also depleted by PC, but restored by ADT (figure 3F,H).

Collectively, these results indicate that both PC and ADT have an impact on the microbiota, which in turn influences the anticancer effects of ADT.

Thymic and microbial effect of ADT in PC patients

Next, we analyzed a cohort of PC patients (online supplemental figure S3 and table S1) with respect to thymus-relevant and microbial parameters. Comparisons of HSPC patients (before or after ADT) with individuals that have developed CRPC (and hence have been subjected to long-term ADT until therapeutic failure) revealed that CRPC was coupled to a reduction in circulating lymphocytes (figure 4A) but an increase in naïve $CD4^+$ T cells (phenotype: $CD45RA^+CD127^+CCR7^+$) (figure 4B) as well as signal-joint T cell receptor excision cycles (sjTREC) indicating enhanced thymic output under ADT (figure 4C). Metagenomic shotgun sequencing of the fecal microbiota detected significant differences in the intestinal ecosystems between HSPC and CRPC patients with an expansion of some anticancer immune response-associated species including *Alistipes*,[49] *Roseburia faecis* ([50]) and *Ruminococcus*[51] under ADT (figure 4D,E) that were lost in the PC mouse model. The overall variance of the microbiota was best explained by the patient status (HSPC

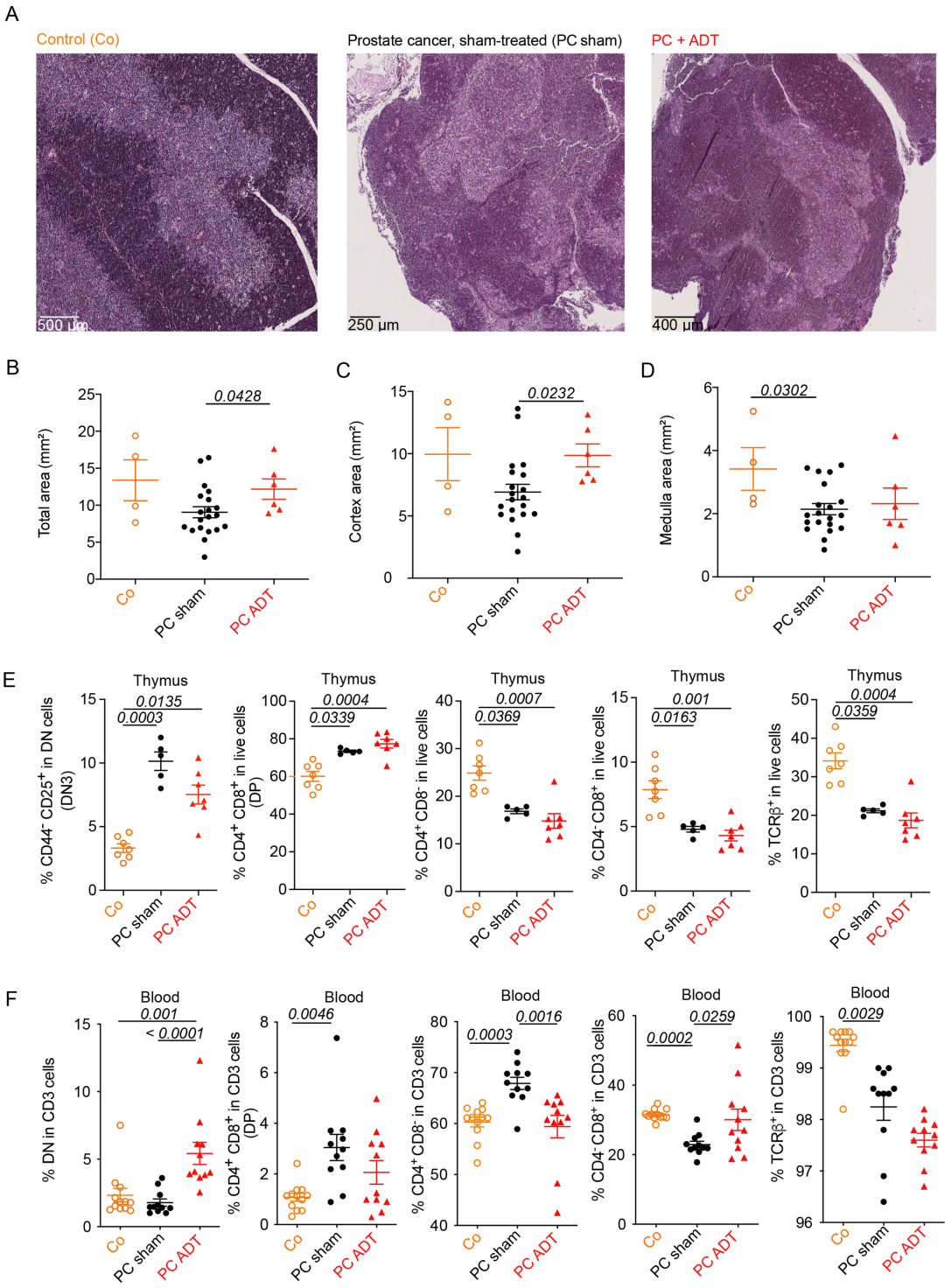

Figure 2 Thymic effect of prostate cancer (PC) and ADT in mice. (A) Micrograph pictures of thymi in naïve and PC tumor-bearing mice treated with ADT. From the left to the right: hematoxylin eosin-stained thymi sections from healthy controls (CO), sham-treated PC bearing mice (PC sham), and ADT -treated PC bearing mice (PC +ADT), sacrificed at D10 post-treatment (scale bars are indicated in the graphs). (B–D). Surface assessment of overall, cortex and medulla areas in the three groups described in (A). Each dot represents one thymus. (E) Flow cytometry determination of thymocyte phenotypes at D10 post -treatment. from left to right: proportion of DN3 thymocytes ($CD44^-CD25^+$ in dn), DP thymocytes ($CD3^+CD4^+CD8^+$), sp $CD4^+$ and $CD8^+$, and $TCR\beta^+$in live cells (F). Flow cytometry determination of circulating lymphocytes at D10 post-treatment. From left to right: proportion of dn in $CD3^+$ cells, DP thymocytes ($CD3^+CD4^+CD8^+$), sp $CD4^+$ and $CD8^+$, and $TCR\beta^+$ in $CD3^+$ cells. Means±SEM are depicted for 4–12 mice/group. A representative experiment is depicted for all graphs except (F) where a pool of two experiments is shown. ANOVA statistical analyses (Kruskal-Wallis test) were used for multiple comparisons. ADT, androgen deprivation therapy; ANOVA, analysis of variance.

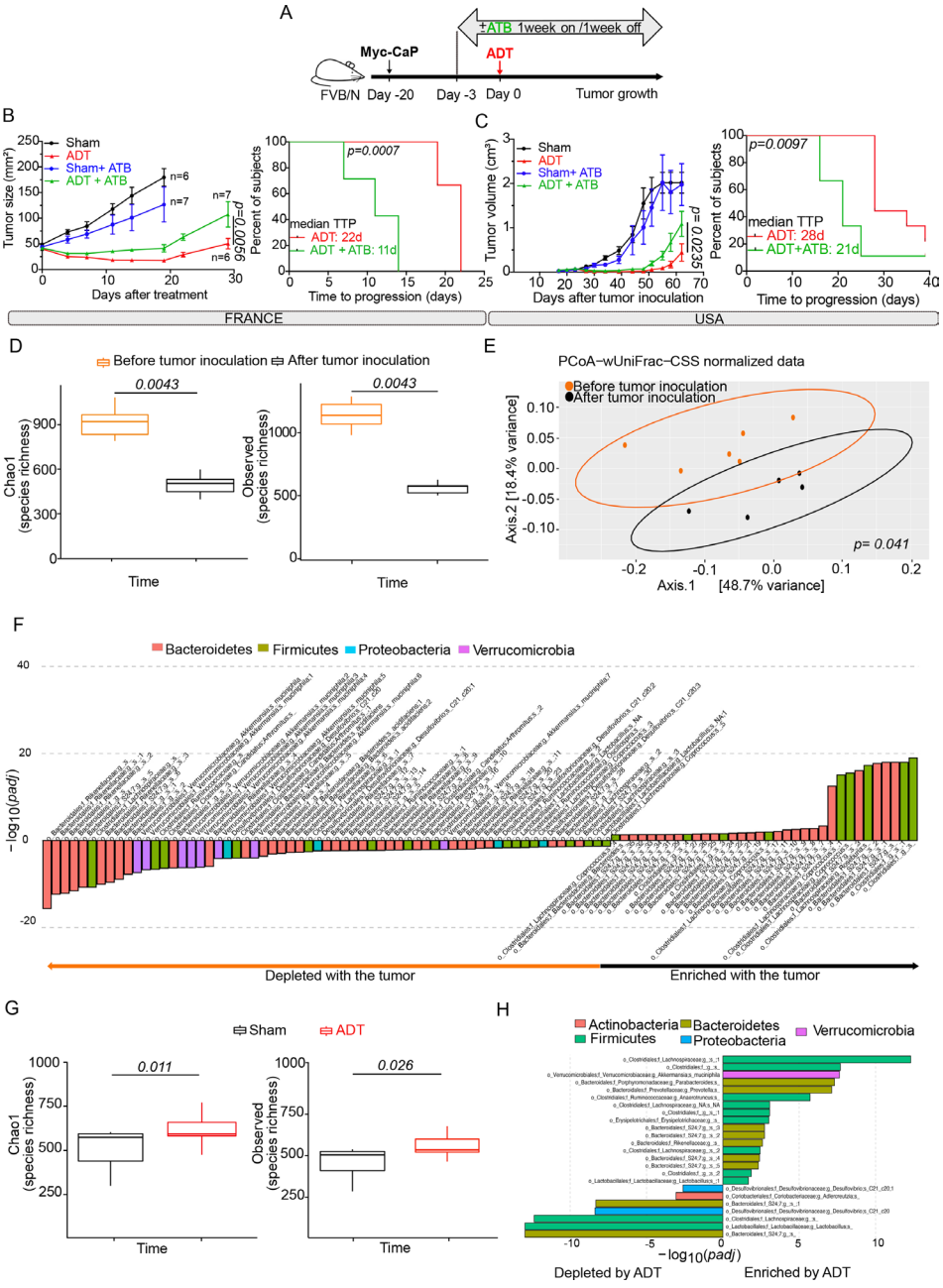

Figure 3 Relationship between ADT and gut microbiota in mice. (A) Experimental setup of Myc-CaP tumor-bearing mice treated with ADT or sham control in the presence or absence of broad-spectrum antibiotics (ATB). ATB were delivered 3 days before ADT and then, 1 week on/1 week off. (B, C) Tumor growth kinetics and TTP in the French animal facility (B) duplicated in a second independent US animal facility (C). (D) Richness of the microbiota intestinal ecosystem estimated by two different methods monitoring the alpha diversity of stools in a longitudinal and paired mouse follow-up, in samples collected before and after tumor inoculation. (E) Beta-Diversity ordination plot based on principal coordinate analysis of normalized and standardized fecal microbiota composition in paired animals before (red dots) and after (black dots) Myc-CaP inoculation. Bray-Curtis distance and weighted UniFrac distance were used as beta diversity metrics and visualized through NMDS method. (F) Bar plots of fecal species that discriminate taxonomic composition between pretumor and post-tumor inoculation in mice by DESeq2 method. (G) Idem as in (D) before and 7 days after ADT. (H) Idem as in (F) pre-ADT and post-ADT in mice. Results were confirmed in two independent experiments; one representative experiment being shown. Tumor growth curves are depicted by means±SEM of tumor sizes over time and P values were calculated using two-way ANOVA for paired repeated measures. Kaplan-Meier curves were used for TTP. The Mann-Whitney U test and the Wilcoxon signed-rank test were used to determine significant differences among the different groups according to alpha-diversity. ADT, androgen deprivation therapy; ANOVA, analysis of variance; CSS, cumulative sum scaling; NMDS, non-metric multidimensional scaling; TTP, time to progression.

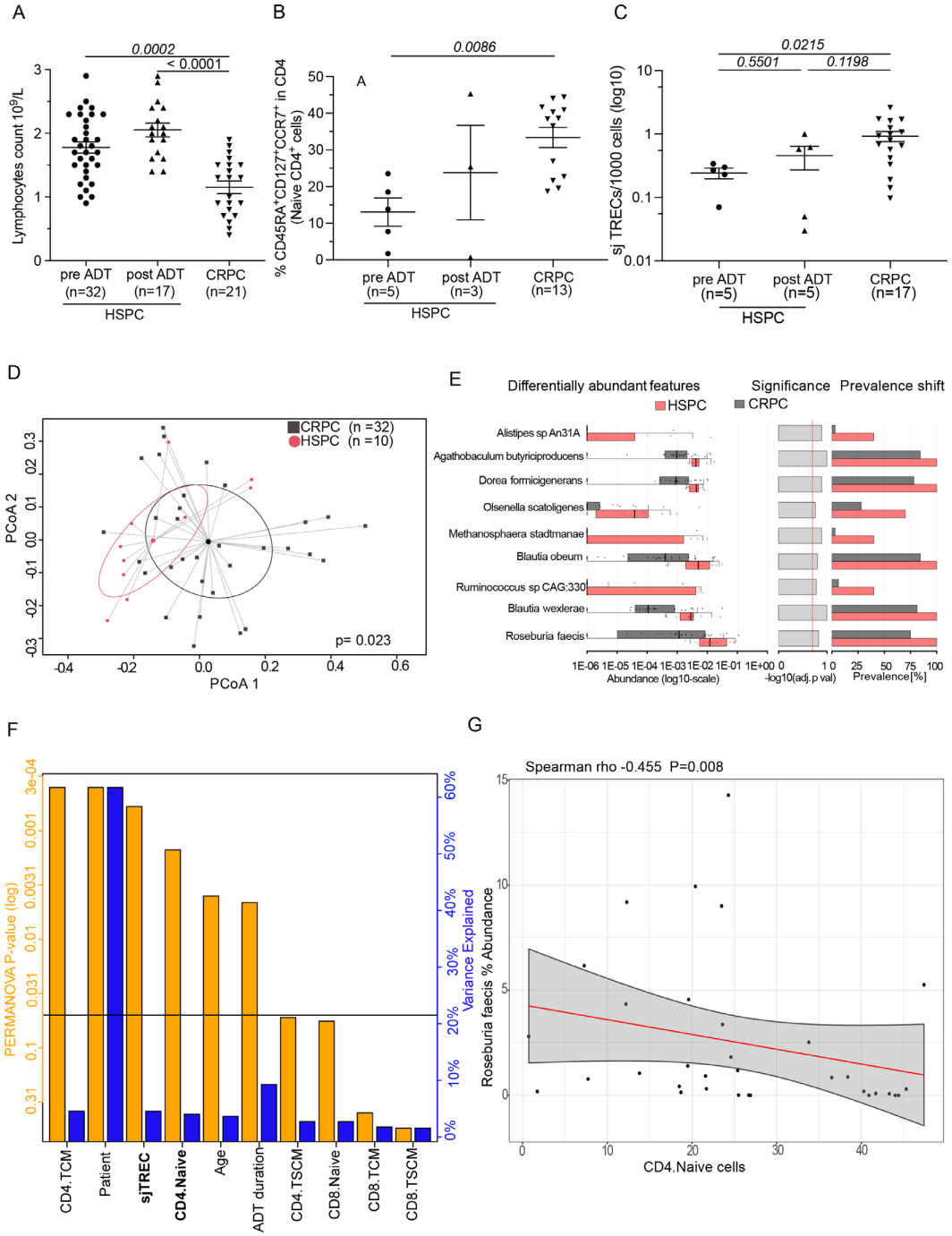

Figure 4 Thymic and microbial effect of ADT in prostate cancer patients. (A) Routine blood monitoring of lymphocyte counts. Absolute blood lymphocyte counts in patients with HSPC at baseline (pre-ADT) and 4–6 months after ADT (post-ADT) as well as in patients with CRPC. (B, C) Flow cytometric determination of blood cell populations. Naïve CD4 +cell proportion (B) and circulating sj TREC cells (C) in patients with (HSPC) pre-ADT and 4–6 months post-ADT and in CRPC patients compared with age-matched and sex-matched healthy controls. (A–C). Each dot represents one patient. The graph depicts means±SEM of lymphocyte counts. ANOVA statistical analyses (Kruskal-Wallis test) were used for multiple comparison. (D–F) Patient fecal microbiota composition and flow cytometry-based blood analysis. Principal coordinate analysis (PcoA) using Bray-Curtis distances calculated using species level relative abundances in CRPC (dark gray dots) and HSPC patients (red dots) (D) prevalence and relative abundances of differentially abundant species between CRPC and HSPC patients (E). Associations between the overall microbial community composition and flow cytometry-based blood analyses (F). Spearman's correlations between immune cell profiles and species' abundances controlling for time-point, age and patient (G). ADT, androgen deprivation therapy; ANOVA, analysis of variance; CRPC, castration-resistant prostate cancer; HSPC, hormone-sensitive PC.

vs CRPC) but also correlated with several immune parameters (in particular the frequency of naïve $CD4^+$ T cells, sjTRECs, but also $CD4^+$ T cells with a central memory (TCM) phenotype: $CD45RA^-CCR7^+CD27^+$) and clinical parameters (patient age and ADT duration) (figure 4F). At the individual species level, the abundance of the health-associated *Roseburia faecis* was negatively associated with the frequency of circulating naïve $CD4^+$ T cells (figure 4G).

Altogether, these results validate the preclinical results at the patient level. PC and ADT cause interlinked alterations in the microbiota and the immune system, and ADT induces the export of thymocytes resulting in an increase in naïve $CD4^+$ T cells in peripheral blood.

Microbial improvement of ADT effects in mice

In the final step of this study, we investigated whether the microbial shifts induced by PC and ADT favor the progression from HSPC to CRPC. In an initial round of experiments, all mice in the same cage were inoculated with PC cells or, alternatively, only half of the mice received PC cells, meaning that these PC-bearing mice were cohoused with tumor-free mice (figure 5A). Cohousing reduced initial PC growth (figure 5B), suggesting that environmental factors including the microbiota (which is transferred between mice due to their coprophagic behavior)[52] have a major impact on PC progression. To evaluate the influence of cohousing on the efficacy of ADT, we subjected mice with established PC to cohousing with cancer-free mice and later ADT (figure 5C). In this context, cohousing improved tumor growth control, enhanced TTP and increased overall survival of PC-bearing mice (figure 5D). Moreover, cohousing plus ADT improved the histological appearance of thymic architecture, divided into a morphologically distinct cortex and medulla, with a clear separation at the corticomedullary junction (figure 5E) and fully corrected the PC-induced increase in DN3 and DP thymocytes (figure 5F,G), as well as the depletion of SP and $TCR\beta^+$ thymocytes (figure 5H–J). Finally, cohousing induced major microbial shifts, including a relative enrichment in *Ruminococcus spp* (figure 5K), which is reputed for its stimulatory effects on tumor immunosurveillance[47 48 53] and has been found to be increased in PC patients under ADT.[41] In sum, transfer of the microbiota from tumor-free to PC-bearing mice had a major positive impact on PC-induced perturbations of the thymus and ameliorated the therapeutic efficacy of ADT.

Of note, the transfer of feces from two PC-bearing patients (one with HSPC and one with CRPC, PC1 and PC2, respectively) accelerated the growth of PC in mice. In contrast, feces from two healthy volunteers (HV1, HV2) failed to affect PC growth as compared with normal mice housed in specific pathogen-free conditions (figure 6A–C) Fecal microbial transplantation of HV1 and HV2 (but not that of PC1 and PC2) also increased the efficacy of ADT (figure 6D).

Importantly, the gavage of mice with *Akkermansia* (*Akkp2261*) enhanced the efficacy of ADT against PC (figure 6E,F) and normalized the frequency of DN3 cells in the thymus (figure 6G) as well as the number of circulating immature T cells (phenotype: $CD3^+TCR\beta^-$) (figure 6H). Also, changes have been noticed in thymus weight and cellularity under microbiota manipulation conditions (cohousing or oral administration of Akkermansia (online supplemental file 3).

Taken together, these results suggest that the microbiota from healthy mice or humans, as well as specific health-associated bacteria such as *A. muciniphila*, impact the immune system and ameliorate the efficacy of ADT in preclinical models.

DISCUSSION

This study unravels the existence of a network of relationships between PC, ADT, thymus-dependent T lymphocytes and the intestinal microbiota. In several cases these relationships cannot be interpreted to represent a hierarchical order but instead are bilateral or even multilateral. For instance, the relationship between PC and the cellular immune system is non-hierarchical. On one hand, PC is under immunosurveillance, meaning that PC evolves and relapses following ADT more quickly in athymic *nu/nu* mice or after antibody-mediated depletion of T lymphocytes. However, in line with a previous study on PC,[54] PC appears to induce thymic atrophy, and ADT reverses selective features of this PC-induced effect. Thus, PC induced a β-TCR deficiency probably related to a TCR rearrangement defect, consistent with the maturation block at the DN3 stage. Indeed, in mice with targeted mutations in the recombinase-activating gene or the TCRβ gene, DN thymocytes pass the $CD44^+CD25^\pm$ stage (DN1 and DN2), and development is blocked at the $CD44^-CD25^+$ stage (DN3).[55] Thus, our results suggest that PC compromises TCRβ chain rearrangement and consequently β-selection leading to a maturation blockage. Of note, ADT ultimately favored a surge of DN T cells in the blood from mice, as well as an increase in naïve $CD4^+$ T cells in patients, that might reflect an increase in thymic output. In accord with this speculation, CRPC patients that had undergone prolonged ADT manifested an increase in recent thymic emigrants positive for sjTREC. Altogether, it appears that PC and its treatment by ADT affect the immune system in opposite manners and that thymus-dependent T cells are involved in the control of PC progression from HSPC to CRPC.

Yet another example of a non-hierarchical, bilateral relationship concerns the mutual influence between PC and the gut microflora. On one hand, the presence of PC apparently alters the microbiota (with the depletion of beneficial bacteria including *A. muciniphila* and *Lachnospiraceae*), and ADT reverses these effects, as found in our preclinical studies, echoing prior clinical reports that ADT enriches *A. muciniphila* in the gut from PC patients.[39 40] On the other hand, normalization

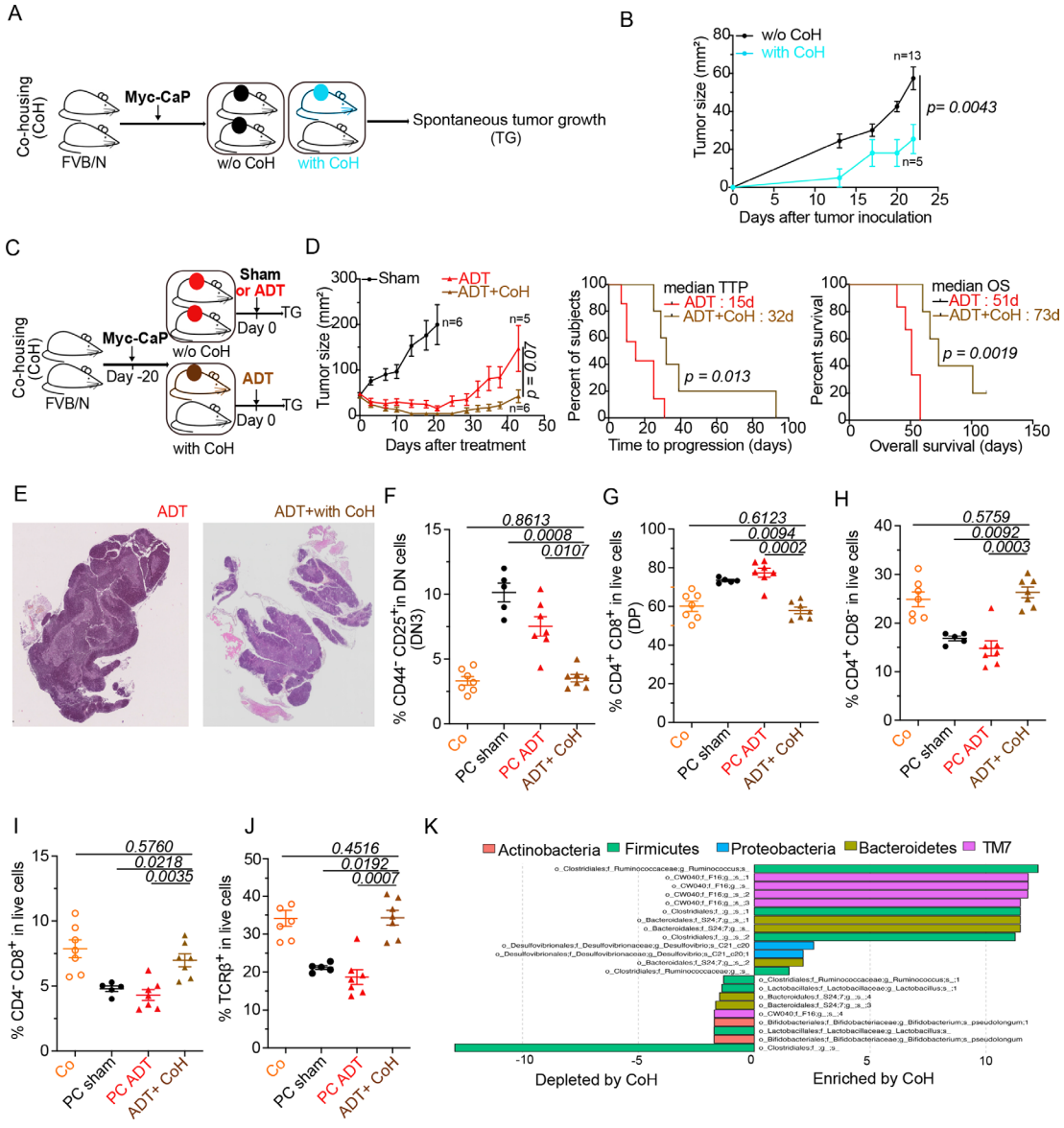

Figure 5 Co-housing (CoH) improved ADT-mediated taxonomic composition of the intestinal ecosystem and anticancer effects. (A–C) Experimental setup of cohousing experiments where tumor-bearing mice were housed with naive littermates prior to (A) or after (C) treatment with ADT. (B–D) Spontaneous and ADT-mediated tumor growth kinetics and TTP with and without cohousing and ADT (D). (E) Idem as in figure 2A. Representative animal for each micrograph picture: left and right panel (without and with cohousing) at D10 post-ADT. Bar scale: 200 mm. (F–J) Flow cytometric determination of thymocytes. proportion of DN3 thymocytes ($CD44^{-}CD25^{+}$ in dn) (F) DP thymocytes ($CD3^{+}CD4^{+}CD8^{+}$) (G) sp $CD4^{+}$ thymocytes (H) sp $CD8^{+}$ thymocytes (I) and $TCR\beta^{+}$in live cells (J). (K) Idem as in figure 3H where metagenomic species discriminating between ADT-treated cohoused and non-cohoused mice. Tumor growth curves are depicted showing means±SEM of tumor sizes over time and p values were calculated using two-way ANOVA for paired repeated measures. Kaplan Meier curves were used for TTP and OS. A typical experiment comprizing at least 5 males/group is depicted, out of 2–3 experiments conducted and yielding similar conclusions. ADT, androgen deprivation therapy; ANOVA, analysis of variance; OS, overall survival; TTP, time to progression.

of the PC-driven microbial shifts can be achieved by three different methods: (1) cohousing with cancer-free mice, (2) fecal microbiota transplantation using the natural product of human volunteers (but not PC patients), and (3) oral administration of *Akkermansia*. These three manipulations reduce PC growth and/or improve the efficacy of ADT against PC, retarding the progression from HSPC to CRPC.[56] We used oral administration of live *Akkermansia* to improve the outcome of ADT. It remains to be determined whether these effects involve adjuvant effects (perhaps mediated by the stimulation of Toll-like receptor two by the protein Amuc_1100),[57] metabolic effects (that may be mediated by a bacterial protein resembling glucagon-like peptide-1 or alternatively by an increase in PPARα agonistic mono-palmitoyl-glycerol and immunostimulatory polyamines)[58–60] or a yet-to-be-discovered cross-reactivity between bacterial and tumor antigens. Indeed, a recent study reports that intravenous injection of *A. muciniphila*-derived extracellular vesicles can

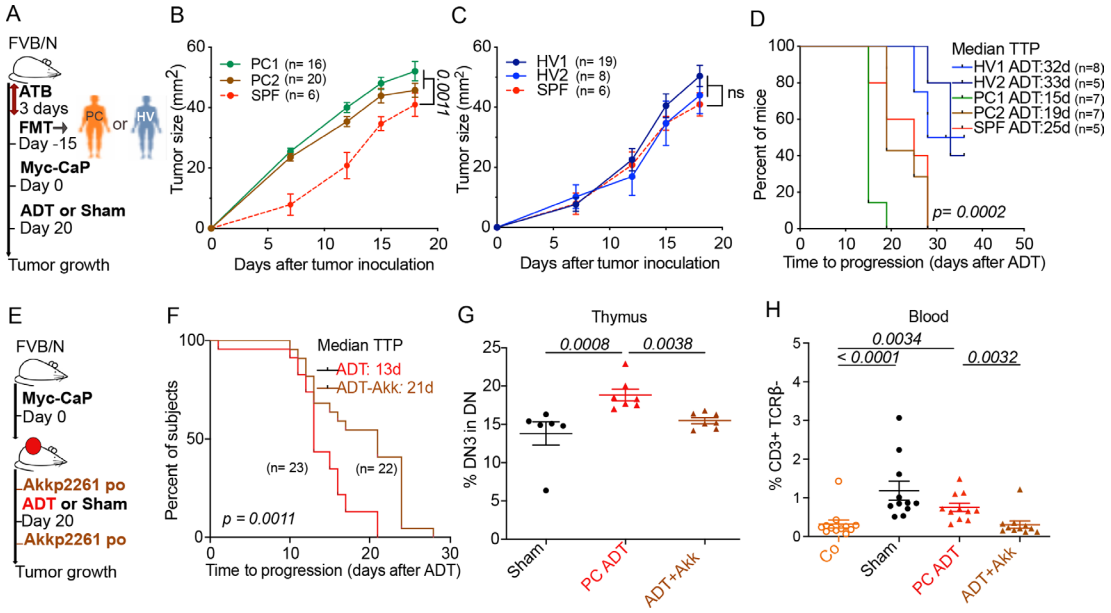

Figure 6 Improving ADT antitumor effects using FMT or *Akkermansiap2261* (Akkp2261) (A) Experimental setup of FMT of stool samples from hormone sensitive patient (PC1) and CRPC patient (PC2) and 2 healthy volunteers (HV1 and HV2). (B) ADT-induced tumor growth after FMT from hormone sensitive patient (PC1) and CRPC patient (PC2) compared with mice without FMT under SPF conditions. (C) Idem as in (B) using FMT from healthy volunteers (HV1 and HV2). (D) TTP Kaplan-Meier curves post-ADT in different FMT arms (PC1, PC2, HV1, HV2, SPF). (E) Experimental setup using oral administration of Akkp2261 or PBS vehicle just before and next after ADT. (F) TTP Kaplan-Meier curves post-ADT with or without Akkp2261. (G–H) Flow cytometric determination of thymic (G) and blood lymphocytes (H) at day 10 post-ADT. Proportion of DN3 thymocytes ($CD44^-$ $CD25^+$ in DN) and blood $CD3^+$ $TCR\beta^-$ δ^- in three different groups: sham control, ADT without and with *A. muciniphila*. Results from one representative experiment out of two or a pool of two experiments are shown. At least five mice per experimental condition. Each dot represents one animal. P values were calculated using two-way ANOVA for paired repeated measures. Kaplan-Meier curves were used for TTP and OS. ADT, androgen deprivation therapy; ANOVA, analysis of variance; CRPC castration-resistant prostate cancer; FMT, fecal microbiota transplantation; OS, overall survival; SPF, specific pathogen-free; PBS, phosphate-buffered saline; TTP, time to progression.

induce $CD8^+$ cytotoxic T cells responses against mouse PC established in immunocompetent C57BL/6 mice that slow down tumor growth in the absence of ADT.[61] At this point, the mechanisms explaining how PC and its hormonal treatment affect the gut microflora or vice versa are mostly elusive. Recent data reported that the intestinal commensal microbiota in mice and patients with CRPC were enriched for species having the ability to convert precursors into active androgens.[56]

There is some evidence suggesting that the relationship between the gut microbiota and the immune system may be reciprocal as well. The immune system controls the homeostasis of the microbiota as well as the inflammatory status of the gut wall, while the microflora controls local and systemic immune responses[62–64] including those involved in cancer immunosurveillance.[34–38] Accordingly, when PC-bearing mice receiving ADT were cohoused with cancer-free mice, the shift to a more normal intestinal microflora was accompanied by an improvement of thymic architecture, as well as restoration of normal thymopoiesis. Moreover, in a heterogeneous cohort of PC patients comprizing both HSPC and CRPC, the variations in the gut microbiota correlated with the abundance of sjTREC, suggesting a functional link between the intestinal ecosystem and thymic output. The mechanistic underpinnings of such a hypothetical link remain to be elucidated.

It should be noted that our work diverges from that recently published by Pernigoni *et al*[56] in several points. Indeed, the work by Pernigoni *et al*[56] postulated that antibiotic-mediated elimination of the gut microbiota may improve the outcome of ADT against PC by eliminating bacteria that produce androgens, thus annihilating the effects of ADT. However, there are several important methodological differences between our study and that by Pernigoni *et al*.[56] First, Pernigoni *et al*[56] used an antibiotic association of neomycin, ampicillin, vancomycin and metronidazole. In our study, we used a different antibiotic cocktail including ampicillin, streptomycin, and colistin without vancomycin. We have accumulated data to show that vancomycin depletes immunosuppressive bacteria such as *Clostridia spp*[65], suggesting that this point is indeed crucial. Second, Pernigoni *et al*[56] performed surgical castration (which is rarely used in the treatment of human PC), while we used chemical castration with an LHRH antagonist (Degarelix). Third, Pernigoni *et al*[56] used the murine TRAMP C1 model, syngeneic from C57BL/6 mice while we focused on the Myc-CaP model growing in FVB/N mice. Altogether, these multiple differences (at (1) the levels of antibiotic cocktails, (2)

treatments to induced ADT and (3) preclinical models) preclude a direct comparison of our study with that by Pernigoni *et al*.[56]

In conclusion, within the uncertainties of experimental and translational oncology, our work reveals that both the immune system and the intestinal microflora determine the efficacy of ADT against PC. Although immunotherapy with immune checkpoint inhibitors targeting CTLA-4 and PD-1 fails to improve ADT, the restoration of a healthy gut microbiota may constitute a valid strategy for prolonging tumor control by ADT.

Author affiliations
[1]INSERM U1015, Gustave Roussy, Villejuif, France
[2]Medical Oncology, Hôpital Saint-Louis, Paris, France
[3]Department of Urology, Kurume University School of Medicine, Kurume, Japan
[4]Department CIBIO, University of Trento, Trento, Italy
[5]Parean Biotechnologies, Saint Malo, France
[6]Institut de Recherche de Paris, INSERM UMRS-1160, Université de Paris, Paris, France
[7]UW Carbone Cancer Center, Madison, Wisconsin, USA
[8]Université Paris-Saclay, Saint-Aubin, France
[9]Gustave Roussy, Villejuif, France
[10]EverImmune Gustave Roussy Cancer Center, Villejuif, France
[11]Center of Clinical Investistigations in Biotherapies of Cancer (CICBT), Villejuif, France
[12]Département de Médicine, CHUM, Montreal, Québec, Canada
[13]Department of Radiation Oncology, Gustave Roussy, Villejuif, France
[14]CRCHUM, Montreal, Québec, Canada
[15]Université de Paris, Paris, France
[16]Department of Biology and Medical Pathology, Gustave Roussy, Villejuif, France
[17]Institut de Recherche Saint Louis, INSERM U1160, Université de Paris, Paris, France
[18]Laboratoire d'immunologie et d'histocompatibilité, Hôpital Saint-Louis, Paris, France
[19]Medicine, University of Wisconsin Madison, Madison, Wisconsin, USA
[20]Department of Medical Oncology, Gustave Roussy, Villejuif, France
[21]Sorbonne Université INSERM U1138, Université de Paris, Paris, France
[22]Gustave Roussy Cancer Campus, Villejuif, France
[23]Université Paris-Saclay Faculté de Médecine, Le Kremlin-Bicetre, France

Twitter Andrew Maltez Thomas @andrew_m_thomas and Emmanuel Clave @ClaveEmmanuel

Acknowledgements We thank Dr. Charles G. Drake (Department of Hematology/Oncology, Columbia University Medical Center, New York, USA) for providing MycCaP cell lines and are grateful for his advices. We thank all members of Gustave Roussy Animal facility.

Contributors LZ, GK, ST: designed, performed, involved in experiment analysis, writing the manuscript, access to the data and controlled the decision to publish. KF: designed, included patients, provided patient clinical data. AGG: involved in the design and in the analysis of mice and human experiments. KU: involved in the performance and analysis of mice experiments. LD: involved in the design and mice experiments. AMT, NS, FA, FP, FA: performed the metagenomics and bio-informatic analysis of human specimens. VQ, HP: performed the bio-informatic analysis of murine experiments. CR, BR: involved in bio-informatic and stastical analysis. GD, AS, FG: Flow cytometry in human specimens. CT,GF, PL, MGH, DGM, CR, CACS, JEF, MM: involved in mice experiments. MF: involved in statisctics and figures design. RD, EP: involved in bacterial manipulations and culture. EC and AT: performed human sj trecs experiment. SY, PO: Pathological analysis. SC, PB: Patients and clinical data.

Funding ST was supported by a Poste d' accueil INSERM fellowship (Plan Cancer). LZ laboratory was supported by the Germano-French ANR Ileobiome - 19-CE15-0029-01 and H2020 ONCOBIOME No 825410, RHU Torino Lumière ANR-16-RHUS-0008; Seerave Foundation; SIRIC Stratified Oncology Cell DNA Repair and Tumor Immune Elimination (SOCRATE). GK is supported by the Ligue contre le Cancer (équipe labellisée); Agence Nationale de la Recherche (ANR)—Projets blancs; AMMICa US23/CNRS UMS3655; Association pour la recherche sur le cancer (ARC); Association 'Ruban Rose'; Cancéropôle Ile-de-France; Fondation pour la Recherche Médicale (FRM); a donation by Elior; Equipex Onco-Pheno-Screen; European Joint Program on Rare Diseases (EJPRD); Gustave Roussy Odyssea, the European Union Horizon 2020 Projects Oncobiome and Crimson; Fondation Carrefour; Institut National du Cancer (INCa); Inserm (HTE); Institut Universitaire de France; LabEx Immuno-Oncology (ANR-18-IDEX-0001); the Leducq Foundation; the and SIRIC Cancer Research and Personalized Medicine (CARPEM). This study contributes to the IdEx Université de Paris ANR-18-IDEX-0001. AMT and EC are supported by the French Government's Investissement d'Avenir Program, Laboratoire d'Excellence "Milieu Intérieur" Grant ANR-10-LABX-69-01. INSERM U.1160 is a member of OPALE Carnot Institute, The Organization for Partnerships in Leukemia. MG-H and DGM are supported by the grant funding NIH/NCI P01 CA250927.

Competing interests LZ and GK are scientific cofounders of everImmune, a company that develops bacteria for the treatment of cancer. GK is a scientific cofounder of Samsara Therapeutics and Therafast Bio. Acknowledgments: LZ laboratory was supported by the Germano-French ANR Ileobiome—19-CE15-0029-01 and H2020 ONCOBIOME N°825410, RHU Torino Lumière ANR-16-RHUS-0008; Seerave Foundation; SIRIC Stratified Oncology Cell DNA Repair and Tumor Immune Elimination (SOCRATE). GK is supported by Agence Nationale de la Recherche (ANR)—Projets blancs; AMMICa US23/CNRS UMS3655; Association pour la recherche sur le cancer (ARC); Association 'Ruban Rose'; Cancéropôle Ile-de-France; Fondation pour la Recherche Médicale (FRM); a donation by Elior; Equipex Onco-Pheno-Screen; European Joint Programme on Rare Diseases (EJPRD); Gustave Roussy Odyssea, the European Union Horizon 2020 Projects Oncobiome and Crimson; Fondation Carrefour; Institut National du Cancer (INCa); Inserm (HTE); Institut Universitaire de France; LabEx Immuno-Oncology (ANR-18-IDEX-0001); the Leducq Foundation; the and SIRIC Cancer Research and Personalized Medicine (CARPEM). This study contributes to the IdEx Université de Paris ANR-18-IDEX-0001. AMT and EC are supported by the French Government's Investissement d'Avenir Program, Laboratoire d'Excellence 'Milieu Intérieur' Grant ANR-10-LABX-69-01. INSERM U.1160 is a member of OPALE Carnot Institute, The Organization for Partnerships in Leukemia. MG-H and DGM are supported by the grant funding NIH/NCI P01 CA250927.

Patient consent for publication Consent obtained directly from patient(s)

Ethics approval This study involves human participants and was approved by Gustave Roussy Cancer Campus, France in 'Oncobiotics' clinical study, B2M ethics protocol number PP: 15-013. Written informed consent in accordance with the Declaration of Helsinki was obtained from all patients. Participants gave informed consent to participate in the study before taking part.

Provenance and peer review Not commissioned; externally peer reviewed.

Data availability statement Data are available in a public, open access repository. The metagenomes have been deposited in NCBI under the bioproject PRJNA791751. Once public, they will be accessible using this link: https://www.ncbi.nlm.nih.gov/bioproject/791751.

ORCID iDs
Safae Terrisse http://orcid.org/0000-0002-9138-2272
Emmanuel Clave http://orcid.org/0000-0001-8217-5039
Melissa Gamat-Huber http://orcid.org/0000-0003-2943-8156
Nicola Segata http://orcid.org/0000-0002-1583-5794
Douglas G McNeel http://orcid.org/0000-0003-1471-6723
Karim Fizazi http://orcid.org/0000-0002-6068-9474

REFERENCES

1 Beyer K, Moris L, Lardas M, *et al*. Diagnostic and prognostic factors in patients with prostate cancer: a systematic review protocol. *BMJ Open* 2021;11:e040531.
2 Tong D. Unravelling the molecular mechanisms of prostate cancer evolution from genotype to phenotype. *Crit Rev Oncol Hematol* 2021;163:103370.
3 Lokeshwar SD, Klaassen Z, Saad F. Treatment and trials in non-metastatic castration-resistant prostate cancer. *Nat Rev Urol* 2021;18:433–42.
4 Schmidt KT, Huitema ADR, Chau CH, *et al*. Resistance to second-generation androgen receptor antagonists in prostate cancer. *Nat Rev Urol* 2021;18:209–26.
5 Flammiger A, Bayer F, Cirugeda-Kühnert A, *et al*. Intratumoral T but not B lymphocytes are related to clinical outcome in prostate cancer. *APMIS* 2012;120:901–8.
6 Davidsson S, Ohlson A-L, Andersson S-O, *et al*. CD4 helper T cells, CD8 cytotoxic T cells, and FOXP3(+) regulatory T cells with respect to lethal prostate cancer. *Mod Pathol* 2013;26:448–55.
7 Ness N, Andersen S, Valkov A, *et al*. Infiltration of CD8+ lymphocytes is an independent prognostic factor of biochemical failure-free survival in prostate cancer. *Prostate* 2014;74:1452–61.
8 Nardone V, Botta C, Caraglia M, *et al*. Tumor infiltrating T lymphocytes expressing FOXP3, CCR7 or PD-1 predict the outcome of prostate cancer patients subjected to salvage radiotherapy after biochemical relapse. *Cancer Biol Ther* 2016;17:1213–20.
9 Yang Y, Attwood K, Bshara W, *et al*. High intratumoral $CD8^+$ T-cell infiltration is associated with improved survival in prostate cancer patients undergoing radical prostatectomy. *Prostate* 2021;81:20–8.
10 Hanahan D, Weinberg RA. The hallmarks of cancer. *Cell* 2000;100:57–70.
11 Hanahan D, Weinberg RA. Hallmarks of cancer: the next generation. *Cell* 2011;144:646–74.
12 Galluzzi L, Humeau J, Buqué A, *et al*. Immunostimulation with chemotherapy in the era of immune checkpoint inhibitors. *Nat Rev Clin Oncol* 2020;17:725–41.
13 Petroni G, Buqué A, Zitvogel L, *et al*. Immunomodulation by targeted anticancer agents. *Cancer Cell* 2021;39:310–45.
14 Casares N, Pequignot MO, Tesniere A, *et al*. Caspase-dependent immunogenicity of doxorubicin-induced tumor cell death. *J Exp Med* 2005;202:1691–701.
15 Obeid M, Panaretakis T, Joza N, *et al*. Calreticulin exposure is required for the immunogenicity of gamma-irradiation and UVC light-induced apoptosis. *Cell Death Differ* 2007;14:1848–50.
16 Humeau J, Sauvat A, Cerrato G, *et al*. Inhibition of transcription by dactinomycin reveals a new characteristic of immunogenic cell stress. *EMBO Mol Med* 2020;12:e11622.
17 Le Naour J, Liu P, Zhao L, *et al*. A TLR3 ligand Reestablishes chemotherapeutic responses in the context of FPR1 deficiency. *Cancer Discov* 2021;11:408–23.
18 Senovilla L, Galluzzi L, Marino G, *et al*. Immunosurveillance against cancer-associated hyperploidy. *Oncotarget* 2012;3:1270–1.
19 Bezu L, Gomes-de-Silva LC, Dewitte H, *et al*. Combinatorial strategies for the induction of immunogenic cell death. *Front Immunol* 2015;6:187.
20 Pfirschke C, Engblom C, Rickelt S, *et al*. Immunogenic chemotherapy sensitizes tumors to checkpoint blockade therapy. *Immunity* 2016;44:343–54.
21 Kroemer G, Galluzzi L, Kepp O, *et al*. Immunogenic cell death in cancer therapy. *Annu Rev Immunol* 2013;31:51–72.
22 Zitvogel L, Rusakiewicz S, Routy B, *et al*. Immunological off-target effects of imatinib. *Nat Rev Clin Oncol* 2016;13:431–46.
23 Liu P, Zhao L, Pol J, *et al*. Crizotinib-induced immunogenic cell death in non-small cell lung cancer. *Nat Commun* 2019;10:1486.
24 Buqué A, Bloy N, Perez-Lanzón M, *et al*. Immunoprophylactic and immunotherapeutic control of hormone receptor-positive breast cancer. *Nat Commun* 2020;11:3819.
25 Drake CG, Doody ADH, Mihalyo MA, *et al*. Androgen ablation mitigates tolerance to a prostate/prostate cancer-restricted antigen. *Cancer Cell* 2005;7:239–49.
26 Page ST, Plymate SR, Bremner WJ, *et al*. Effect of medical castration on CD4+ CD25+ T cells, CD8+ T cell IFN-gamma expression, and NK cells: a physiological role for testosterone and/or its metabolites. *Am J Physiol Endocrinol Metab* 2006;290:E856–63.
27 Mercader M, Bodner BK, Moser MT, Kwon PS, *et al*. T cell infiltration of the prostate induced by androgen withdrawal in patients with prostate cancer. *Proc Natl Acad Sci U S A* 2001;98:14565–70.
28 Gamat M, McNeel DG. Androgen deprivation and immunotherapy for the treatment of prostate cancer. *Endocr Relat Cancer* 2017;24:T297–310.
29 Sorrentino C, Musiani P, Pompa P, *et al*. Androgen deprivation boosts prostatic infiltration of cytotoxic and regulatory T lymphocytes and has no effect on disease-free survival in prostate cancer patients. *Clin Cancer Res* 2011;17:1571–81.
30 Zitvogel L, Perreault C, Finn OJ, *et al*. Beneficial autoimmunity improves cancer prognosis. *Nat Rev Clin Oncol* 2021;18:591–602.
31 Pearce P, Khalid BA, Funder JW. Androgens and the thymus. *Endocrinology* 1981;109:1073–7.
32 Aspinall R, Andrew D. Gender-Related differences in the rates of age associated thymic atrophy. *Dev Immunol* 2001;8:95–106.
33 Mittelbrunn M, Kroemer G. Hallmarks of T cell aging. *Nat Immunol* 2021;22:687–98.
34 Zitvogel L, Ma Y, Raoult D, *et al*. The microbiome in cancer immunotherapy: diagnostic tools and therapeutic strategies. *Science* 2018;359:1366–70.
35 Finlay BB, Goldszmid R, Honda K, *et al*. Can we harness the microbiota to enhance the efficacy of cancer immunotherapy? *Nat Rev Immunol* 2020;20:522–8.
36 Baruch EN, Wang J, Wargo JA. Gut microbiota and antitumor immunity: potential mechanisms for clinical effect. *Cancer Immunol Res* 2021;9:365–70.
37 Fluckiger A, Daillère R, Sassi M, *et al*. Cross-reactivity between tumor MHC class I-restricted antigens and an enterococcal bacteriophage. *Science* 2020;369:936–42.
38 Sepich-Poore GD, Zitvogel L, Straussman R, *et al*. The microbiome and human cancer. *Science* 2021;371. doi:10.1126/science.abc4552. [Epub ahead of print: 26 03 2021].
39 Sfanos KS, Markowski MC, Peiffer LB, *et al*. Compositional differences in gastrointestinal microbiota in prostate cancer patients treated with androgen axis-targeted therapies. *Prostate Cancer Prostatic Dis* 2018;21:539–48.
40 Daisley BA, Chanyi RM, Abdur-Rashid K, *et al*. Abiraterone acetate preferentially enriches for the gut commensal Akkermansia muciniphila in castrate-resistant prostate cancer patients. *Nat Commun* 2020;11:4822.
41 Wang LL, Wong CYP. A cross-sectional study on gut microbiota in prostate cancer patients with prostatectomy or androgen deprivation therapy. *Prostate Cancer Prostatic Dis* 2021.
42 Watson PA, Ellwood-Yen K, King JC, *et al*. Context-dependent hormone-refractory progression revealed through characterization of a novel murine prostate cancer cell line. *Cancer Res* 2005;65:11565–71.
43 Marangoni E, Vincent-Salomon A, Auger N, *et al*. A new model of patient tumor-derived breast cancer xenografts for preclinical assays. *Clin Cancer Res* 2007;13:3989–98.
44 Venkatachalam S, McFarland TR, Agarwal N, *et al*. Immune checkpoint inhibitors in prostate cancer. *Cancers* 2021;13. doi:10.3390/cancers13092187. [Epub ahead of print: 02 05 2021].
45 Sharma P, Pachynski RK, Narayan V, *et al*. Nivolumab plus ipilimumab for metastatic castration-resistant prostate cancer: preliminary analysis of patients in the CheckMate 650 trial. *Cancer Cell* 2020;38:489–99.
46 Vétizou M, Pitt JM, Daillère R, *et al*. Anticancer immunotherapy by CTLA-4 blockade relies on the gut microbiota. *Science* 2015;350:1079–84.
47 Routy B, Gopalakrishnan V, Daillère R, *et al*. The gut microbiota influences anticancer immunosurveillance and general health. *Nat Rev Clin Oncol* 2018;15:382–96.
48 Gopalakrishnan V, Spencer CN, Nezi L, *et al*. Gut microbiome modulates response to anti-PD-1 immunotherapy in melanoma patients. *Science* 2018;359:97–103.
49 Iida N, Dzutsev A, Stewart CA, *et al*. Commensal bacteria control cancer response to therapy by modulating the tumor microenvironment. *Science* 2013;342:967–70.
50 Tamanai-Shacoori Z, Smida I, Bousarghin L, *et al*. Roseburia spp.: a marker of health? *Future Microbiol* 2017;12:157–70.
51 Daillère R, Vétizou M, Waldschmitt N, *et al*. Enterococcus hirae and Barnesiella intestinihominis facilitate cyclophosphamide-induced therapeutic immunomodulatory effects. *Immunity* 2016;45:931–43.
52 Shabat Y, Lichtenstein Y, Ilan Y. Short-Term Cohousing of sick with healthy or treated mice alleviates the inflammatory response and liver damage. *Inflammation* 2021;44:518–25.
53 Cascone T, William WN, Weissferdt A, *et al*. Neoadjuvant nivolumab or nivolumab plus ipilimumab in operable non-small cell lung cancer: the phase 2 randomized NEOSTAR trial. *Nat Med* 2021;27:504–14.
54 Borodin YI, Lomshakov AA, Astashov VV, *et al*. Thymus in experimental carcinogenesis of the prostate gland. *Bull Exp Biol Med* 2014;157:724–7.
55 Mombaerts P, Clarke AR, Rudnicki MA, *et al*. Mutations in T-cell antigen receptor genes alpha and beta block thymocyte development at different stages. *Nature* 1992;360:225–31.

56 Pernigoni N, Zagato E, Calcinotto A, *et al*. Commensal bacteria promote endocrine resistance in prostate cancer through androgen biosynthesis. *Science* 2021;374:216–24.
57 Plovier H, Everard A, Druart C, *et al*. A purified membrane protein from Akkermansia muciniphila or the pasteurized bacterium improves metabolism in obese and diabetic mice. *Nat Med* 2017;23:107–13.
58 Depommier C, Vitale RM, Iannotti FA, *et al*. Beneficial effects of Akkermansia muciniphila are not associated with major changes in the circulating Endocannabinoidome but linked to higher Mono-Palmitoyl-Glycerol levels as new PPARα agonists. *Cells*2021;10:185.
59 Grajeda-Iglesias C, Durand S, Daillère R, *et al*. Oral administration of *Akkermansia muciniphila* elevates systemic antiaging and anticancer metabolites. *Aging* 2021;13:6375–405.
60 Yoon HS, Cho CH, Yun MS, *et al*. Akkermansia muciniphila secretes a glucagon-like peptide-1-inducing protein that improves glucose homeostasis and ameliorates metabolic disease in mice. *Nat Microbiol* 2021;6:563–73.
61 Wu Q, Tian A-L, Li B, *et al*. IGF1 receptor inhibition amplifies the effects of cancer drugs by autophagy and immune-dependent mechanisms. *J Immunother Cancer* 2021;9:e002722.
62 Elinav E, Strowig T, Kau AL, *et al*. NLRP6 inflammasome regulates colonic microbial ecology and risk for colitis. *Cell* 2011;145:745–57.
63 Ivanov II, Atarashi K, Manel N, *et al*. Induction of intestinal Th17 cells by segmented filamentous bacteria. *Cell* 2009;139:485–98.
64 López-Otín C, Kroemer G. Hallmarks of health. *Cell* 2021;184:33–63.
65 Yonekura S, Terrisse S, Alves Costa Silva C, *et al*. Cancer induces a stress ileopathy depending on B-adrenergic receptors and promoting dysbiosis that contribute to carcinogenesis. *Cancer Discov* 2021. doi:10.1158/2159-8290.CD-21-0999. [Epub ahead of print: 20 Dec 2021].

MATERIALS AND METHODS

I. Human study

1. Patient characteristics

French cohort of patients with prostate cancer

Stool metagenomic analysis: 32 Patients with CRPC (castration refractory prostate cancer) and 10 Patients with HSPC (hormone sensitive prostate cancer) were enrolled at Gustave Roussy Cancer Campus, France in "Oncobiotics" clinical study, B2M ethics protocol number PP: 15-013 (see flow diagram of patient inclusion Figure S3). Written informed consent in accordance with the Declaration of Helsinki was obtained from all patients. Samples were collected at baseline, before treatment initiation regardless of the treatment line.

Blood samples: 27 paired blood samples were also collected from previous patients, 17 CRPC and 10 HSPC (5 pre-ADT and 5 post-ADT) in Oncobiotics clinical study.

Lymphocyte count analysis: We retrospectively collected lymphocyte count for 21 mCRPC from Oncobiotics study (ethics protocol number PP: 15-013) and 31 hormone sensitive patients from PEACE ONE (NCT01957436), LATTITUDE (NCT01715285) studies at the Gustave Roussy site and standard of care patients.

The lymphocyte count was collected at baseline before treatment with androgen deprivation therapy (GNRH agonists or antagonists) for the 32 patients and paired 17 patients at 4-6 months after ADT initiation.

2. Sequence preprocessing and taxonomic profiling:

DNA have been extracted with Qiagen DNeasy PowerSoil Pro Kit following the manufacture's instruction.

Sequencing libraries were prepared using the Illumina Nextera DNA Flex Library Prep Kit according to manufacturer's protocols. Libraries were multiplexed using dual

indexing and sequenced for 300 bp paired-end reads using the Illumina NovaSeq6000 platform according to manufacturer's protocols. All sequenced metagenomes were QCed using the pre-processing pipeline implemented in https://github.com/SegataLab/preprocessing. This pre-processing pipeline consists of three main stages: **(1)** Initial quality control by removing low-quality reads (quality score <Q20), fragmented short reads (<75 bp), and reads with >2 ambiguous nucleotides; **(2)** contaminant DNA removal by using Bowtie2 and the --sensitive-local parameter, removing both the phiX174 Illumina spike-in and human-associated reads (hg19); **(3)** Sorting and splitting for the creation of standard forward, reverse, and unpaired reads output files for each metagenome. We obtained an average of 76,823,598 reads/sample after quality control and pre-processing. Taxonomic profiling and quantification of organisms' relative abundances of all metagenomic samples was performed using MetaPhlAn 3.0 (F. Beghini et al) with default parameters.

3. Stastistics:

Exploratory analysis of β-diversity was calculated using the Bray-Curtis measure of dissimilarity on species-level relative abundances and represented in Principal Coordinate Analyses (PCoA). P-values were determined by using 10,000 permutations in the function adonis from the vegan R package (v2.5-7). Non-parametric Wilcoxon tests were used for univariate differential abundance analysis using SIAMCAT (J.Wirbel et al.) after abundance filtering. Spearman’s correlations between immune cell profiles and species’ abundances were computed using the pcor.test function from the ppcor R package controlling for time-point, age and patient. P values were

corrected using false discovery rate (FDR) through the Benjamini-Hochberg procedure.

4. Quantification of T-cell Receptor (TCR) Excision Circles (TRECs):

TREC quantification was performed as in Clave et al. (E. Clave et al.). Briefly, real time quantification was made using ViiA7 (Applied Biosystems by Life Technologies, Austin, TX, USA) in 384-well plates loaded with 20 µl containing 500 ng of genomic DNA,1x Takyon Low Rox Probe MM (Eurogentec) and 200 nM sjTREC LNA probe (FAM-ACACCTCTGGTTTTTGTAAAGGTG-EclipseDQ with N= LNA base), 100 nM Alb probe VIC-CCTGTCATGCCCACACAAATCTCTCC-TAMRA, 400 nM sjTREC-F CACATCCCTTTCAACCATGCT, 400 nM sjTREC-R, GCCAGCTGCAGGGTTTAGG, 20 nM ALB-F, GCTGTCATCTCTTGTGGGCTGT and 20 nM ALB-R, ACTCATGGGAGCTGCTGGTTC. All primers and probes are from Eurogentec except the Alb probe from Applied Biosystems. sjTRECs were normalized to 150 000 cells (around 1 µg of DNA) using the Albumin gene quantification. Male aged matched controls are from a 150 healthy adults aged between 19 and 95 years old (Pitié Salpétrière Hospital, Paris) (Nicoli et al, submitted)

5. Flow cytometry analysis:

Preparation.

PBMCs were stained for flow cytometry analysis at +4°C for 20 minutes. Antibodies used for flow cytometry analysis are included in the table below. All stainings were performed using a FACS buffer made with 2% FBS 10 uM EDTA in PBS.

Target	Fluorochrome	Company	Clone	Staining
CD8	Brillant UltraViolet395	BD	RPTA8	Extracellular
CD4	Brillant UltraViolet496	BD	RPTA4	Extracellular
CD45	Brillant UltraViolet563	BD	HI30	Extracellular
CD3	Briallant UltraViolet805	BD	UCHT1	Extracellular
CD279/PD-1	Brillant Violet421	BD	EH12.1	Extracellular
CD45RO	Pacific Blue	BioLegend	UCHL1	Extracellular
CD62L	Brillant Violet480	BD	DREG	Extracellular
TCRδ	Brillant Violet510	BD	11F2	Extracellular
CD25	Brillant Violet605	BD	2A3	Extracellular
CD197/CCR7	Brillant Violet650	BioLegend	G043H7	Extracellular
CD31	Brillant Violet711	BD	L133.1	Extracellular
CD28	Brillant Violet785	BioLegend	CD28.2	Extracellular
Vβ11	FITC	Beckman Coulter	C21	Extracellular
CD44	PerCP/Cyanine5.5	BioLegend	BJ18	Extracellular
CD95	BB700	BD	DX2	Extracellular
TOX1	PE	Miltenyi	REA473	Intracellular
CD127	PE/Cyanine5.5	ThermoFisher	eBioRDR5	Extracellular
Vα24	PE/Dazzle 594	BioLegend	6b11	Extracellular
CD27	PE/Cyanine 7	BioLegend	O323	Extracellular
Foxp3	APC	Thermo Fisher	PCH101	Intracellular
TCF-1	Alexa Fluor 647	BioLegend	7F11A10	Intracellular
CD45RA	Alexa Fluo700	BD	HI100	Extracellular
TCRαβ	APC/Cyanine 7	BD	IP26	Extracellular

Acquisition.

Stained samples were acquired on a CyTEK Aurora flow cytometer (Cytek Biosciences).

Analysis.

Fcs files were exported and analysed using FlowJo software (Tree Star, Ashland, OR, USA) and Prism 9.

II. Pre-clinical study details

1. Mice

All animal experiments were carried out in compliance with French and European laws and regulations. The local institutional animal ethics board and French Ministère de la Recherche approved all mouse experiments (permission numbers: 2018_026_14002). Experiments were performed in accordance with Government and institutional guidelines and regulations.

Immunocompetent mice: for main experiment, FVB/N males were purchased from Charles River (France). Mice were used between 8 and 10 weeks of age. All mouse experiments were performed at the animal facility in Gustave Roussy. Cancer Campus where animals were housed in specific pathogen-free conditions.

Nude-athymic mice were purchased from Gustave Roussy (France).

2. Tumor cell line

Myc-CaP cells, derived from spontaneous prostate cancer in c-Myc transgenic mice, were a generous gift from Dr. Charles. L. Sawyers and were maintained as previously described (Watson, P. A. et al)

3. Animal model

Immunocompetent mice:

FVB/NJ mice were subcutaneously inoculated with Myc-CaP cells (1×10^6 cells/mouse) in the right flank as previously described (Shen, Y.-C. et al). Tumor diameters were measured every 3 days with an electronic caliper. Tumor surface were calculated using the formula: longest diameter × shortest diameter. When tumor surface reached approximately 60 mm^2, mice were randomly allocated to treatment groups as indicated. Euthanasia was performed for tumor ulceration, tumor surface > 300 mm^2, or any other sign of animal suffering. Time to progression is defined as the time between the first treatment and the regrowth of tumor to a size greater than 20 mm2

that was confirmed on 2 successive measurements. Overall survival (OS) was defined as the time period between castration and death.

Immunocompromised mice:

Athymic nude mice lacking T cells were used (nu/nu mice): the same process as described above.

4. Androgen deprivation therapy (ADT)

Androgen deprivation therapy is a subcutaneous (sc) injection of degarelix acetate (a GnRH receptor antagonist; Ferring Pharmaceuticals Inc., Parsippany, NJ) at a dosage of 0.625 mg in 100 µl physiologic serum every 28 days.

5. Immune checkpoint Inhibitors (ICIs)

Five or ten days after ADT, Mice were treated intraperitonaly (ip), with 4 injections of anti-PD-1 mAb (250µg/mouse, clone RMP1-14), anti-CTLA-4 (100µg of anti-CTLA-4 mAb (clone 9D9) or isotype control (clone 2A3 and clone MPC11 respectively) every 3-days.

6. T- Cell depletion

For in vivo depletion of CD4 and CD8 T lymphocytes, we performed i.p. injection of 200 µg/ mice of monoclonal Antibodies (mAbs) or isotype controls. Mice were treated 3 days prior to ADT and then weekly.

We used anti-mouse Abs (clone GK1.5) for CD4 depletion, anti-mouse Abs (clone 53–6.72) for CD8 depletion and isotype controls (LTF-2 and 2A3). All antibodies were from Bioxcell).

The depletion was confirmed after 3 injections by flow cytometric (FC) analysis of blood samples.

7. Antibiotic treatments

Mice were treated with an antibiotic solution (ATB) containing ampicillin (1 mg/ml), streptomycin (5 mg/ml), and colistin (1 mg/ml) (Sigma-Aldrich), added in the drinking

water of mice. Antibiotic activity was confirmed by cultivating fecal pellets suspended in BHI+15% glycerol at 0.1 g/ml on COS (Columbia Agar with 5% Sheep Blood) plates for 48 h at 37°C in aerobic and anaerobic conditions.

In the context of antibiotic induced dysbiosis: mice received 3 days of ATB before ADT and for 14 days, then 1 week on/ 1 week off.

In the context of fecal microbial transplantation experiments: mice received 3 days of ATB before undergoing fecal microbial transplantation the next day by oral gavage using animal feeding needles.

8. Cohousing experiment

We used the cohousing method, a gold standard for the analysis of intestinal microbiota phenotype transfer (Rakoff-Nahoum et al.). Tumour-bearing mice were cohoused with healthy tumour-free mice prior to treatment with ADT.

Animals were randomly assigned to experimental groups (i.e., cohoused or non-cohoused). During cohousing experiments, the investigators were not blinded to allocation during experiments.

9. Fecal microbiota transfer experiments (FMT)

Fecal microbiota transfer (FMT) was performed by thawing fecal material. Two hundred µL of the suspension was then transferred by oral gavage into ATB pre-treated recipient. In addition, another 100µL was applied on the fur of each animal. Two weeks after FMT, tumor cells were injected subcutaneously and mice were treated with ADT or isotype controls with or without oral gavage of fecal samples from responding patients or of commensal species, as mentioned above.

10. Gut colonization with Akkermansia

Akkermansia CSUR P2261 (Akkp2261) was provided by the Institut hospital-universitaire Méditerranée Infection, Marseille, France.

Akkp2261 was grown on COS plates in an anaerobic atmosphere created using 3 anaerobic generators (Biomerieux) at 37°C for at least 72h. Akkp2261 was verified using a Matrix-Assisted Laser Desorption/Ionization Time of Flight (MALDI-TOF) mass spectrometer (Microflex LT analyser, Bruker Daltonics, Germany).

Akkp2261 was inactived by pasteurization (30 min at 70°C) and then immediately frozen and stored at -80°C.

Colonization of mice was performed by oral gavage with 100uL of suspension containing 1x10^8 bacteria. For bacterial gavage: suspension of 10^9 CFU/mL were obtained using a fluorescence spectrophotometer (Eppendorf) at an optical density of 600 mn in NaCl. Two bacterial gavages were performed for each mouse, the first 24h before the androgen deprivation therapy (ADT) and subsequently 6 hours after this injection.

11. Analysis of immunohistochemistry biomarkers.

A slide scanner Olympus VS120 at 20x objectives was used to obtain a whole slide image (WSI). WSIs were imported into QuPath software (version 0.2.0-m8). Total tissue area was calculated using 'Simple Tissue Detection' in QuPath and modified manually. A region of interest (ROI) for cortex area was identified manually or by an algorithm using ImageJ software (version 1.52r). Briefly, green channel of WSIs was extracted and the region of interest (ROI) was calculated by binary threshold defined for each image. The ROI was modified by hand in QuPath software and defined as cortex area. The area of medulla was calculated by deduction of the total area by cortex area.

12. Sequence preprocessing and taxonomic profiling:

DNA extraction and 16S rRNA sequencing of mouse stools. Preparation and sequencing of mouse fecal samples were performed at IHU Méditerranée Infection,

Marseille, France. Briefly, DNA was extracted using two protocols. The first protocol consisted of physical and chemical lysis, using glass powder and proteinase K respectively, then processing using the Macherey-Nagel DNA Tissue Extraction kit (Duren, Germany). The second protocol was identical to the first protocol, with the addition of glycoprotein lysis and deglycosylation steps. The resulting DNA was sequenced, targeting the V3–V4 regions of the 16S rRNA gene as previously described. 16S rRNA gene sequence processing and analysis was performed using R v3.6.1 and GraphPad Prism v8.3.1. DADA2 R package v1.14.0 (B.J Callahan et al.) was used to generate exact amplicon sequence variants (ASV) of each sample from raw amplicon sequences. Sequences were corrected for Illumina amplicon sequence errors, de-replicated, chimera removed, and merged of paired-end reads with 240-bases for forward reads and 220-bases for reverse reads. The taxonomy assignment was performed against the SILVA reference database (v132) (C. Quast et al.). Archea and Eukaryota residual sequences were removed. Alpha-diversity, defined as the number of distinguishable taxa, was analyzed at the genus-level and computed with phyloseq R package26 v1.30.0 (McMurdie PJ, et al.). The alpha-diversity, a mathematical value that summarizes an ecological (e.g. microbial) community according to the count of unique species and how evenly their frequencies are distributed, was estimated with different metrics at the genus-level: observed ASV, Shannon index, Inverse Simpson index, as well as weighted and unweighted Faith's Phylogenetic Diversity. Bray–Curtis distance and weighted UniFrac distance were used as beta diversity metrics (which shows the difference in taxonomic abundance profiles from different samples) and visualized through NMDS method (Chengsong Zhu et al.). The Mann–Whitney U test and the Wilcoxon signed-rank test were used to determine significant differences among the different groups according to alpha-

diversity respectively for paired samples. The DESeq2 (Love MI et al.) R package was used to performed differential abundances analysis at the genus-level.

13. Flow cytometry analyses:

Tissues processing

Myc-CaP Tumors. Sub-cutaneous tumors were harvested at D20-D28. Excised tumors were cut into small pieces and digested in RPMI medium containing LiberaseTM at 25 µg/mL (Roche) and DNase1 at 150 UI/mL (Roche) for 30 minutes at 37°C and then crushed and filtered twice using 70 and 40 µm cell strainers (Becton & Dickinson).

Thymus: Thymus were mechanically disaggregated and passed into a sterile filter (40 µm) then rinsed with RPMI and centrifuged. The pellets were resuspended in 2 mL of complete media.

For both organs, the total count was established with Vi-Cell (Beckmann Coulter).

Flow cytometry

Preparation

Depending on the timepoint of the experiment (tumor size and treatment), from one to ten million of cells from tumor samples were used. Five million of thymocytes were stained in each experiment. Cells were pre-incubated with purified anti-mouse CD16/CD32 (1 µg per test, clone 93; eBioscience) and viability marker (1:100 per test, Zombie Aqua™ Fixable Viabikity Kit, BioLegend) for 10 minutes at +4°C in PBS 1X, before membrane staining. Cells were then stained with a panel of extracellular antibodies (see below) for 20 minutes at +4°C. Samples were washed, fixed and permeabilized (Foxp3/Transcription Factor Staining Buffer Set eBiosciences) for 40 min at +4°C before being stained with intracellular antibodies (see below) for 30 min at +4°C. Intracellular and extracellular labelling were performed in FACS buffer made with 2% FBS 10 uM EDTA in PBS. Cells were pre-incubated with a viability marker

(LIVE/DEAD™ Fixable Blue Dead Cell Stain Kit, ThermoFisher) for 20 minutes at +4°C in PBS 1X, before membrane staining.

Target	Fluorochrome	Company	Clone	Staining	Tissue
CD25	Pacific Blue	BioLegend	PC61	extracellular	Tumor and Thymus
CD3	Brillant Violet 650	BD	145-2C11	extracellular	Tumor and Thymus
CD44	PerCP/Cyanine 5.5	BioLegend	IM7	extracellular	Tumor and Thymus
CD45	APC-R700	BD	30-F11	extracellular	Tumor
CD8a	PE	eBiosciences	53-6.7	extracellular	Tumor and Thymus
CD4	PE/Dazzle 594	BioLegend	GK1.5	extracellular	Tumor and Thymus
CD4	PerCP/Cyanine 5.5	BioLegend	GK1.5	extracellular	Tumor
CD137/4-1BB	PE	BioLegend	17B5	extracellular	Tumor
CD366/TIM 3	PE/Dazzle 594	BioLegend	B8.2C12	extracellular	Tumor
CD8	PE-Cy7	BioLegend	53-6.7	extracellular	Tumor
CD183/CX CR3	APC	eBiosciences	173	extracellular	Tumor
CD45	Alexa Fluor 700	BioLegend	104	extracellular	Tumor
CD3	APC/Cyanine7	BD	145-2C11	extracellular	Tumor
CD279/PD-1	Brillant Violet421	BioLegend	RMP1-30	extracellular	Tumor
CD223/LA G3	Brillant Violet650	BioLegend	C9B7W	extracellular	Tumor
CD152/CT LA4	Brillant Violet605	BioLegend	UC10-4B9	intracellular	Tumor
TCRβ	APC/Cyanine7	BioLegend	H57-597	extracellular	Thymus
TCRδ	APC	eBiosciences	eBioGL3	extracellular	Thymus

Acquisition:

Stained samples were acquired on a Cytoflex (Beckman Coulter) cytometer.

Analysis

Fcs files were exported and analysed using FlowJo software (Tree Star, Ashland, OR, USA), R Studio and Prism.

Blood Flow cytometry :

Red blood cell was lysed with ACK, a cocktail of 8,29g of chlorure of amonium, 0,037g of ethyl diamine tetraacetic acid, 1g of bicarbonate of potassium and water. Cells was resuspended in FACS Buffer and stained with a mix of anti-mouse antibodies (same as thymus panel above).

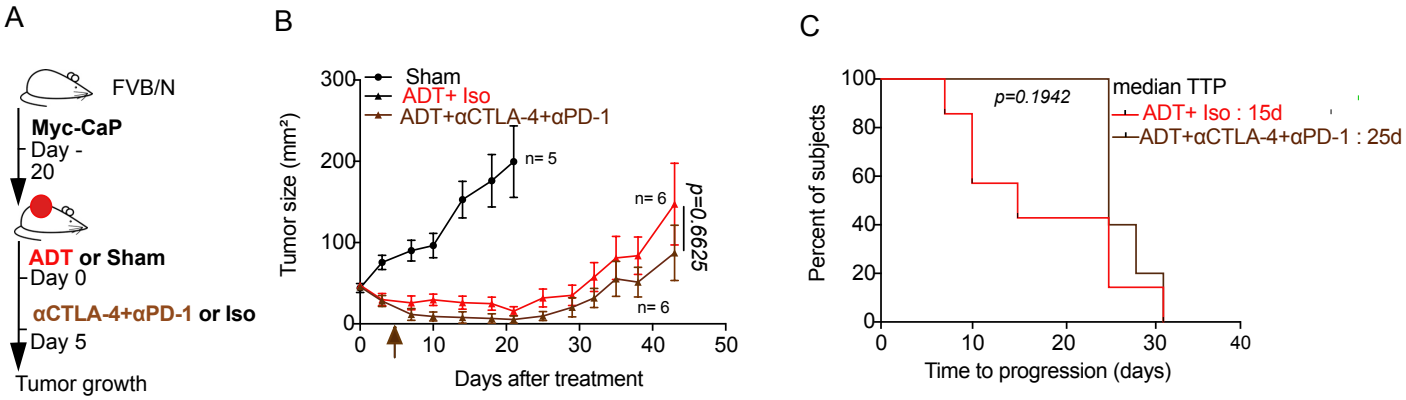
A
FVB/N
Myc-CaP
Day -
20
ADT or Sham
Day 0
αCTLA-4+αPD-1 or Iso
Day 5
Tumor growth
B
Sham
ADT+ Iso
ADT+αCTLA-4+αPD-1
Tumor size (mm²)
n= 5
n= 6
n= 6
p=0.6625
Days after treatment
C
p=0.1942
median TTP
ADT+ Iso : 15d
ADT+αCTLA-4+αPD-1 : 25d
Percent of subjects
Time to progression (days)

Fig S1.

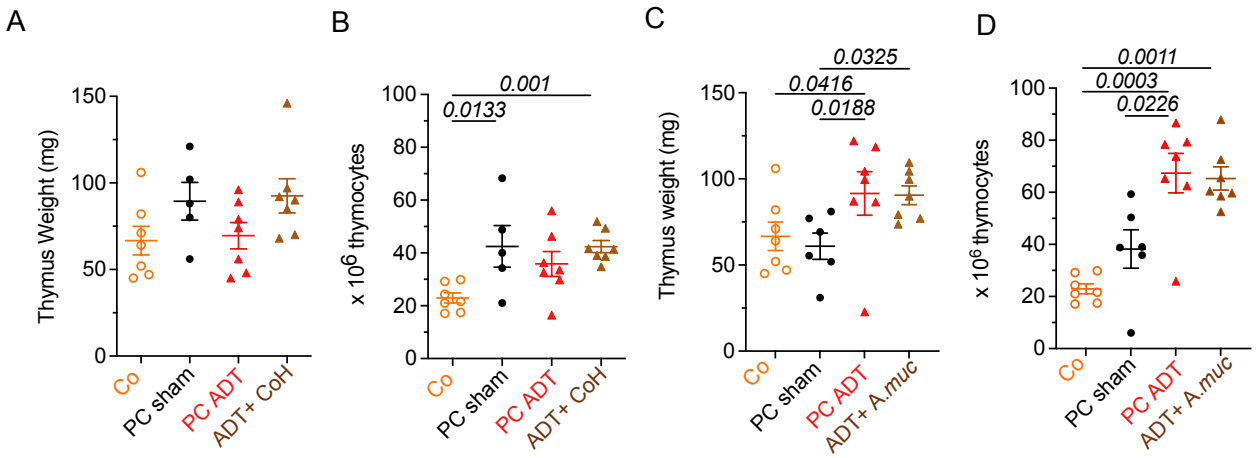
A
Thymus Weight (mg)
150
100
50
0
Co
PC sham
PC ADT
ADT+ CoH
B
x 10^6 thymocytes
100
80
60
40
20
0
0.001
0.0133
Co
PC sham
PC ADT
ADT+ CoH
C
Thymus weight (mg)
150
100
50
0
0.0325
0.0416
0.0188
Co
PC sham
PC ADT
ADT+ A.muc
D
x 10^6 thymocytes
100
80
60
40
20
0
0.0011
0.0003
0.0226
Co
PC sham
PC ADT
ADT+ A.muc

Fig. S2

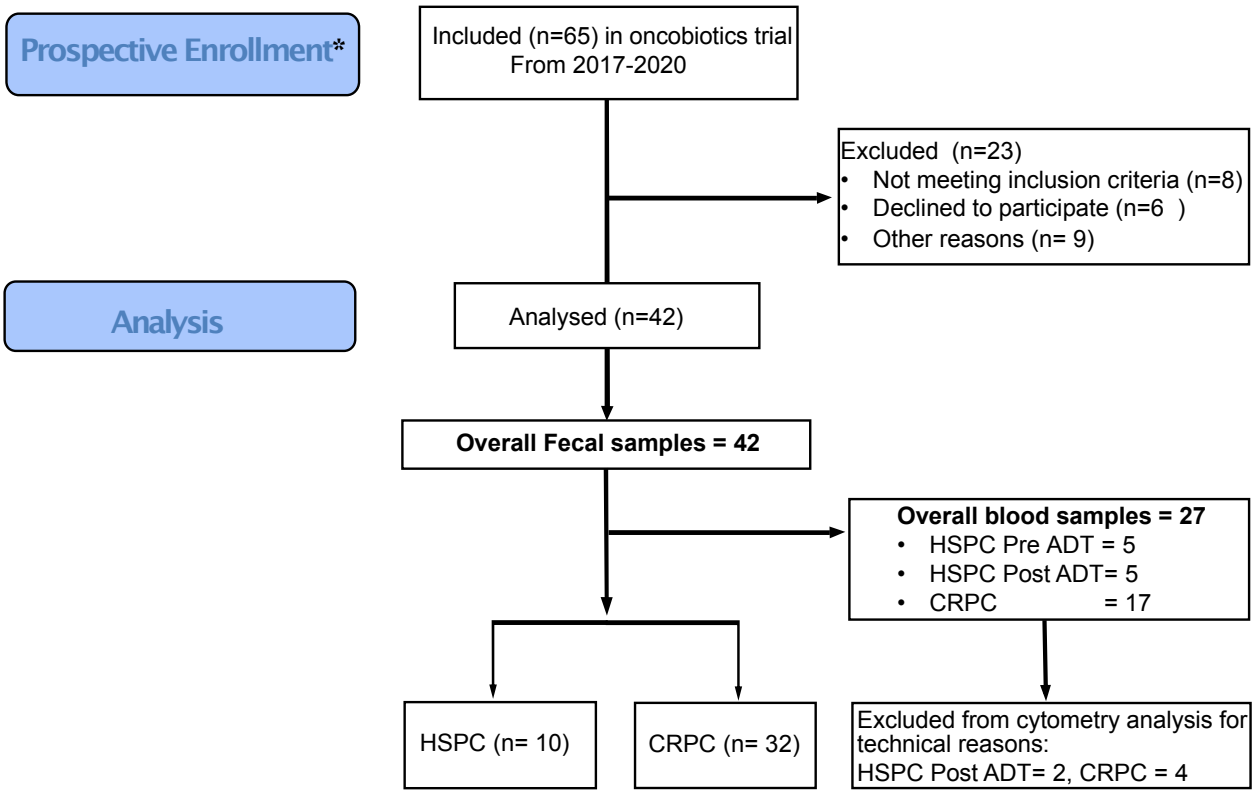

HSPC: hormone-sensitive prostate cancer, CRPC: castration-resistant prostate cancer, ADT: androgen deprivation therapy.
*Lymphocytes count in the fig. 4A, was extracted from different trials (cf materials and methods): n=70, HSPC pre ADT: 32, post ADT: 17 and CRPC: 21 patients.

Fig. S3

Patients characteristics	**CRPC**		**HSPC**	
n		**35**		**10**
Age, mean (Min, Max)		71 (58, 91)		70 (57, 79)
PS, n (%)	0	14 (40)		8 (80%)
	1	21 (60)		2 (20%)
Metastasic (%)		35 (100)		6 (60%)
	Bone	35 (100)	High risk	1 (16.6%)
	Visceral	0	Low risk	5 (83.4%)
Localized (%)		0		4 (40%)
Number of prior systemic cancer therapy, n (%)	0	19 (54.3)		-
	≥ 1	16 (45.7)		-
Sample collection timing, n (%)			V1	10
			V2	3
			V3-V4	8

HSPC: hormone-sensitive prostate cancer, CRPC: castration-resistant prostate cancer, ADT: androgen deprivation therapy. PS: performans status. V1: Baseline pre ADT, V2: short term post ADT (3 weeks), V3-4: long term post ADT (3-6 months).

Table. S1